Rapid spectral-domain localization

Thomas van Dijk,[1] David Mayerich,[1] Rohit Bhargava,[1,2] and P. Scott Carney[1,3]

[1]*Beckman Institute for Advanced Science and Technology, University of Illinois at Urbana-Champaign, USA*
[2]*Department of Bioengineering, University of Illinois at Urbana-Champaign, USA*
[3]*Department of Electrical and Computer Engineering, University of Illinois at Urbana-Champaign, USA*

carney@uiuc.edu

Abstract: We present a method to dynamically image structures at nanometer spatial resolution with far-field instruments. We propose the use of engineered nanoprobes with distinguishable spectral responses and the measurement of coherent scattering, rather than fluorescence. Approaches such as PALM/STORM have relied on the rarity of emission events in time to distinguish signals from distinct probes. By distinguishing signals in the spectral domain, we enable the acquisition of data in a multiplex fashion and thus circumvent the fundamental problem of slow data acquisition of current techniques. The described method has the potential to image dynamic systems with a spatial resolution only limited to the size of the scattering probes.

OCIS codes: (100.6640) Superresolution; (110.4234) Multispectral and hyperspectral imaging.

References and links

1. E. Betzig, G. H. Patterson, R. Sougrat, O. W. Lindwasser, S. Olenych, J. S. Bonifacino, M. W. Davidson, J. Lippincott-Schwartz, and H. F. Hess, "Imaging intracellular fluorescent proteins at nanometer resolution," Science **313**, 1642–1645 (2006).
2. M. J. Rust, M. Bates, and X. Zhuang, "Sub-diffraction-limit imaging by stochastic optical reconstruction microscopy (STORM)," Nat. Methods **3**, 793–795 (2006).
3. S. T. Hess, T. P. K. Girirajan, and M. D. Mason, "Ultra-high resolution imaging by fluorescence photoactivation localization microscopy," Biophys. J. **91**, 4258–4272 (2006).
4. T. D. Lacoste, X. Michalet, F. Pinaud, D. S. Chemla, A. P.Alivisatos, and S. Weiss, "Ultrahigh-resolution multicolor colocalization of single fluorescent probes," Proc. Nat. Acad. Sci. **97**, 9461–9466 (2000).
5. M. Heilemann, D. P. Herten, R. Heintzmann, C. Cremer, C. Müller, P. Tinnefeld, K. D. Weston, J. Wolfrum, and M. Sauer, "High-resolution colocalization of single dye molecules by fluorescence lifetime imaging microscopy," Anal. Chem. **74**, 3511–3517 (2002).
6. P. Lemmer, M. Gunkel, D. Baddeley, R. Kaufmann, A. Urich, Y. Weiland, J. Reymann, P. Müller, M. Hausmann, and C. Cremer, "SPDM: light microscopy with single-molecule resolution at the nanoscale," Appl. Phys. B **93**, 1–12 (2008).
7. E. Abbe, "Beiträge zur theorie des mikroskops und der mikroskopischen wahrnehmung," Arch. Mikroskop. Anat. **9**, 413–418 (1873).
8. F. R. S. Lord Rayleigh, "XXXI. investigations in optics, with special reference to the spectroscope," Phil. Mag. (5) **8**, 261–274 (1879).
9. S. W. Hell, "Far-field optical nanoscopy," Science **316**, 1153–1158 (2007).
10. S. W. Hell and J. Wichmann, "Breaking the diffraction resolution limit by stimulated emission: stimulated-emission-depletion fluorescence microscopy," Opt. Lett. **19**, 780–782 (1994).
11. S. Bretschneider, C. Eggeling, and S. W. Hell, "Breaking the diffraction barrier in fluorescence microscopy by optical shelving," Phys. Rev. Lett. **98** (2007).

#187433 - $15.00 USD Received 20 Mar 2013; revised 2 May 2013; accepted 3 May 2013; published 17 May 2013

12. M. Bates, B. Huang, G. T. Dempsey, and X. Zhuang, "Multicolor super-resolution imaging with photo-switchable fluorescent probes RID d-4854-2009," Science **317**, 1749–1753 (2007).
13. M. S. Gunewardene, F. V. Subach, T. J. Gould, G. P. Penoncello, M. V. Gudheti, V. V. Verkhusha, and S. T. Hess, "Superresolution imaging of multiple fluorescent proteins with highly overlapping emission spectra in living cells," Biophys. J. **101**, 1522–1528 (2011).
14. H. Bock, C. Geisler, C. Wurm, C. von Middendorff, S. Jakobs, A. Schönle, A. Egner, S. Hell, and C. Eggeling, "Two-color far-field fluorescence nanoscopy based on photoswitchable emitters," Appl. Phys. B **88**, 161–165 (2007).
15. M. Heilemann, S. van de Linde, A. Mukherjee, and M. Sauer, "Super-Resolution imaging with small organic fluorophores," Angew. Chem. Int. Ed. **48**, 6903–6908 (2009).
16. I. Testa, C. A. Wurm, R. Medda, E. Rothermel, C. von Middendorf, J. Foelling, S. Jakobs, A. Schoenle, S. W. Hell, and C. Eggeling, "Multicolor fluorescence nanoscopy in fixed and living cells by exciting conventional fluorophores with a single wavelength," Biophys. J. **99**, 2686–2694 (2010).
17. S. Link, Z. L. Wang, and M. A. El-Sayed, "Alloy formation of Gold-Silver nanoparticles and the dependence of the plasmon absorption on their composition," J. Phys. Chem. B **103**, 3529–3533 (1999).
18. S. G. Adie, B. W. Graf, A. Ahmad, P. S. Carney, and S. A. Boppart, "Computational adaptive optics for broadband optical interferometric tomography of biological tissue," Proc. Nat. Acad. Sci. **109**, 7175–7180 (2012).
19. S. G. Adie, N. D. Shemonski, B. W. Graf, A. Ahmad, P. S. Carney, and S. A. Boppart, "Guide-star-based computational adaptive optics for broadband interferometric tomography," Appl. Phys. Lett. **101**, 221117 (2012).
20. C. Guillon, P. Langot, N. Del Fatti, F. Valle, A. S. Kirakosyan, T. V. Shahbazyan, T. Cardinal, and M. Treguer, "Coherent acoustic vibration of metal nanoshells," Nano Lett. **7**, 138–142 (2007).
21. A. K. Kodali, X. Llora, and R. Bhargava, "Optimally designed nanolayered metal-dielectric particles as probes for massively multiplexed and ultrasensitive molecular assays," Proc. Nat. Acad. Sci. **107**, 13620–13625 (2010).
22. M. Pilo-Pais, S. Goldberg, E. Samano, T. H. LaBean, and G. Finkelstein, "Connecting the nanodots: Programmable nanofabrication of fused metal shapes on DNA templates," Nano Lett. **11**, 3489–3492 (2011).
23. Y.-S. Chen, W. Frey, S. Kim, P. Kruizinga, K. Homan, and S. Emelianov, "Silica-coated gold nanorods as photoacoustic signal nanoamplifiers," Nano Lett. **11**, 348–354 (2011). PMID: 21244082.
24. H. C. van de Hulst, *Light scattering by small particles* (Dover Publications, 1982).
25. A. S. Thakor, J. Jokerst, C. Zavaleta, T. F. Massoud, and S. S. Gambhir, "Gold nanoparticles: A revival in precious metal administration to patients," Nano Lett. **11**, 4029–4036 (2011).

We propose a new technique to provide rapid super-resolved mapping of nanoprobes. The method relies on computed localization of isolated probes, analogous to the methods of super-resolution mapping techniques are photoactivation localization microscopy (PALM) [1], stochastic optical reconstruction microscopy (STORM) [2], fluorescence photoactivation localization microscopy (FPALM) [3], referred to collectively here as PALM/STORM. Methods earlier developed in the fluorescence community [4–6] have pointed to the advantages of spectral multiplexing. Rather than isolating individual fluorescent emission events in time, we propose to identify the signal coherently scattered from individual nanoprobes in the spectral domain. We thus overcome the limited temporal resolution of current fluorescence microscopy techniques and bring to bear the advantages of coherent scattering. This dramatically reduces the bandwidth constraint that limits the number of distinguishable probes that can be used in fluorescence-based approaches

Subcellular structures are unresolvable by classical optical techniques as such structures are smaller than the resolution limit, as described by Abbe and Rayleigh [7, 8]. Super-resolved fluorescence microscopy techniques have been developed to overcome this long-standing far-field resolution barrier in recent years [9] and can be divided into two major approaches. One approach relies on a nonlinear optical response to reduce the width of the point spread function either directly or in post-acquisition image synthesis. The best-developed example of such a technique is stimulated-emission-depletion fluorescence microscopy (STED) in which a second laser depletes excited fluorophores that are farthest away from the focal spot [10].

A second approach circumvents the usual resolution limits by transforming imaging into a mapping problem. While imaging is a problem of estimating the components of a vector in an infinite-dimensional Hilbert space, and limited by bandwidth, mapping is a series of problems each requiring an estimate of two or three components of a vector in a two- or three-dimensional

#187433 - $15.00 USD Received 20 Mar 2013; revised 2 May 2013; accepted 3 May 2013; published 17 May 2013

Hilbert space and limited by signal-to-noise ratio (SNR). This reduction in dimensionality of the problem is achieved by limiting the number of active fluorescent probes in the resolved region to one. Switchable fluorescent probes provide such control, enabling separation of individual probes in the time domain from spatially overlapping fluorescent images. For each activated probe the position is calculated by finding the center of the imaged spot. A complete image is subsequently built by acquiring a series of subimages. If the field at the detector from one fluorescent probe is represented as $|s_j\rangle$, the complete field is given by $|S\rangle = \sum_{j=1}^{N} |s_j\rangle$, where N is the total number of probes. The fluorophors are characterized by a source density $\left|\rho_j\right\rangle$. The preparation of the sample is such that only one probe in the resolved region is active at one moment of time, i.e., $\langle \mathbf{r}, t|\rho_j\rangle = \delta^{(3)}(\mathbf{r}-\mathbf{r}_j)\delta(t-t_j)$. Each probes contribution to the field at the detector is a result of the incident field propagating through the optical system and interacting with the sample. Since the system is linear the interaction can be represented by the operator $\mathbf{Q}$ acting on the sample, i.e., $|s_j\rangle = \mathbf{Q}|\rho_j\rangle$. Projecting the total signal onto the temporal basis using the projection operator $\mathbf{T}$ gives

$$\mathbf{T}|S\rangle = \int \mathrm{d}^2 r\, |\mathbf{r}\rangle\langle \mathbf{r}, t|S\rangle = \sum_{j=1}^{j=N} \int \mathrm{d}^2 r\, |\mathbf{r}\rangle\langle \mathbf{r}, t|\mathbf{Q}|\rho_j\rangle. \tag{1}$$

Here, it is assumed that the sample is two dimensional and hence the operator $\mathbf{T}$ maps from $L_2(\mathbb{R}^3)$ to $L_2(\mathbb{R}^2)$. For a non-dispersive system $\mathbf{Q}$ can be represented as

$$\mathbf{Q} = \int \mathrm{d}^2 r \mathrm{d}r' \mathrm{d}t' |\mathbf{r}, t'\rangle Q_{r,r'} \langle \mathbf{r}', t'|. \tag{2}$$

Inserting Eq. (2) into Eq. (1) yields

$$\mathbf{T}|S\rangle = \sum_{j=1}^{N} \int \mathrm{d}^2 r |\mathbf{r}\rangle \delta(t-t_j) Q_{r,r_j}. \tag{3}$$

In general, every system is dispersive; hence contributions from different probes will not be separated in time by simple delta function. However, as long as the dispersion is not so big that is causes overlapping responses this approach still works. Depending on the numerical aperture of the imaging system, the point-spread function, Q_{r,r_j}, will always have a finite width. Finding the location of the fluorescent probe then requires finding the centroid of the image spot.

High-precision mapping of probes was independently implemented as PALM [1], STORM [2],and FPALM [3]. In these techniques, the location of the individual probes can be estimated with a higher precision than the diffraction limit. The sequential localization of the fluorescent probes, builds up the final map over time. The localization precision is proportional to $\propto 1/\sqrt{N_{ph}}$, where N_{ph} is the number of detected photons, which extends measurement times further.

As a consequence of the fact that spatial mapping precision depends on the isolation of emission events in time, the major limiting factor of PALM/STORM methods is the intrinsic trade-off between spatial and temporal resolution, making them slower and less suitable than conventional microscopy for dynamic samples. While spatial resolution may be improved by measuring for a longer period, this leads to a reduced temporal resolution. Applications are therefore mainly limited to static or slowly-changing samples. Strand-like tissue such as microtubules have become a benchmark structure [11–13]. Including fluorescent probes with spectrally distinct emission spectra allows for parallel acquisition and improves imaging times [12–15]. However, these approaches, though spectrally multiplex, still rely on rarity of emission in the time domain and thus require long observations times. To date the number of differently

#187433 - $15.00 USD Received 20 Mar 2013; revised 2 May 2013; accepted 3 May 2013; published 17 May 2013

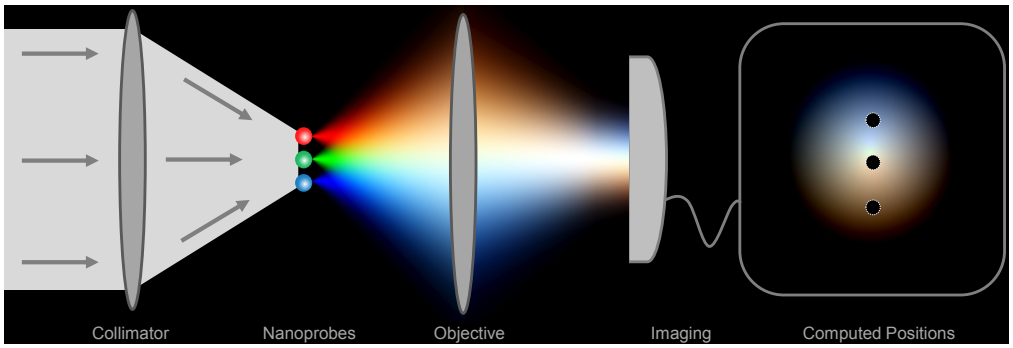

Fig. 1. Illustration of the imaging system. A collection of nanoprobes embedded in a sample placed within the focal volume of the imaging system. The position of the nanoprobes are retrieved using the described method.

colored dyes being imaged simultaneously has been limited to four [16] due to various technological challenges. Hence, resolution in PALM/STORM approaches has reached a practical limit dictated by the intrinsic properties of the process as well as by available technology.

Here we show through theory and simulation that by distinguishing signals in the spectral domain, as illustrated in Fig. 1, the slow data acquisition of current techniques can be overcome. Given a collection of spectrally distinguishable nanoprobes, it is possible to achieve precision mapping with fast measurements and high throughput. Just as in the PALM/STORM approach, the total field at the detector will be given by a sum of contributions from distinct sources that built up the total image, i.e., $|S\rangle = \sum_{j=1}^{j=N} |s_j\rangle$. The sample consists of N nanoprobes, each is denoted by a susceptibility, $|\eta_j\rangle$, rather than a source density, $\left|\rho_j\right\rangle$, as for fluoresence. The signals are multiplexed in the spectral domain and $\langle \mathbf{r},k|\eta_j\rangle = \delta^{(2)}(\mathbf{r}-\mathbf{r}_j)f_j(k)$, here $f_j(k)$ is the spectral response of the individual nanoprobes and $k = \frac{2\pi}{\lambda}$. If the spectral responses of nanoprobes are very narrow and they are well separated then $f_j(k)$ can be approximated by $\delta(k-k_j)$. Projecting the total signal onto the spectral domain, and following similar steps as in the analysis of the PALM/STORM method immediately yields

$$\mathbf{T}|S\rangle = \sum_{j=1}^{N} \int \mathrm{d}^2 r |\mathbf{r}\rangle \delta(k-k_j) Q_{r,r_j}. \tag{4}$$

By selection of the appropriate frequency, k_j, the location of the nanoprobe with that spectral response is found by determining the centroid of Q_{r,r_j}. In general the spectral responses will not be delta-function like but will often overlap. In which case it is necessary to rely on an iterative approach, like nonlinear least-squares regression, to find the locations.

We propose to use the field coherently scattered from nanoprobes of spectrally distinguishable optical response with data collected over short integration times, thus addressing the limitations now seemingly inherent in super-resolved PALM/STORM imaging. Additionally, the use of coherently scattered light provides access to phase information, so it is possible to probe the local refractive index of the sample and perhaps apply computational adaptive optics approaches [18,19] to improve coregistered conventional images. The signal associated with each individual nanoprobe may be obtained by projection of the total signal onto the spectral response of each probe at each pixel in the raw data. The location of each of the probes can be determined by finding the centroid of the projected signal. Since the measurement is not limited by the need to excite probes at low light levels, SNR can be increased by simply increasing the

#187433 - $15.00 USD Received 20 Mar 2013; revised 2 May 2013; accepted 3 May 2013; published 17 May 2013

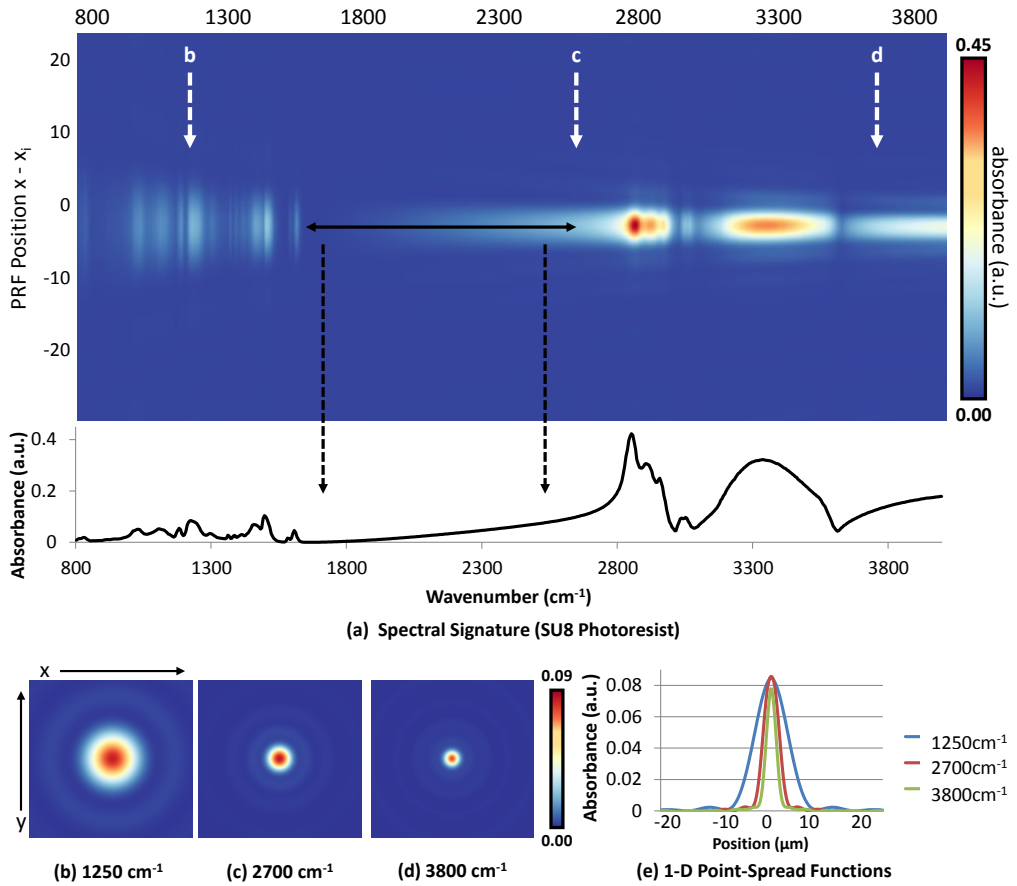

Fig. 2. The spectral-domain particle response function (PRF) is shown for a 1μm sphere composed of SU-8 photoresist and imaged using a mid-infrared spectroscopic microscope. The PRF cross-section is shown in the spectral domain along with the spectrum at the central spatial location (a). Images of the PSF are shown for various wavenumbers (b-d) and the absorbance is plotted as a function of distance from the sphere position (e).

power of the illuminating light up to sample damage threshold.

Obtaining distinct spectral responses for all probes appearing in a single focal volume is the main technological challenge. The required spectral diversity may be engineered by a number of means in coherent scattering. For instance, plasmon resonances can be tuned by controlling the gold-silver ratio in alloy spherical nanoparticles [17] or by nanoscale structuring of the probe [20–23]. Another approach to obtain a wide variety of distinct spectral responses is to rely on unique Raman spectra of ample available Raman molecules. The major disadvantage of Raman imaging is the intrinsically small Raman cross-section which prevents single-molecule detection. To overcome this nanoprobes can be covered with a layer of Raman molecules and can act as a surface-enhanced Raman spectroscopy (SERS) platform.

1. Results and Discussion

As an illustration of a rapid spectral domain super-resolved imaging technique, the coherent scattering of distinct nanospheres is simulated. We first demonstrate that the signal from indi-

#187433 - $15.00 USD Received 20 Mar 2013; revised 2 May 2013; accepted 3 May 2013; published 17 May 2013

vidual nanoprobes may be isolated in the spectral domain even when several probes are located in a single focal volume. This is done by building a forward model based on classical optical theory. Consider the generic far-field imaging system illustrated in Fig. 1 in which a collection of nanoprobes have been embedded in a sample and are illuminated by broad-band radiation. The field is coherently scattered and focused onto a detector plane in the far-zone of the sample. Since the scattered field of a nanoprobe is small and isotropic, it is more convenient to sample the scattered field in reflection. This allows us to eliminate the large incident signal from our detector measurements. Changing the composition of a spherical probe produces a scattered field that can be accurately modeled using Mie theory [24]. The power spectral density of the field is measured on the detector plane as a function of the position $\mathbf{r}$ and wavenumber $k = \frac{2\pi}{\lambda}$. Classical optical theory is used to describe the incident field and the scattered fields produced by nanoprobes of known size and material properties. Scalar fields are described here, but the analysis is readily generalized to vector fields. Consider the case that to a good approximation the field scattered by the nanoparticle is linear in the particle density. The field at the plane of the detector is is represented by the vector $|S\rangle$. The two-dimensional Fourier component of the field at spatial frequency $\mathbf{k}_\parallel$ is given by $\widetilde{S}(\mathbf{k}_\parallel) = \langle \mathbf{k}_\parallel | S \rangle$. The sample is described by the vector $|\eta\rangle$. The field at the detector can then be denoted by

$$|S\rangle = \mathbf{Q}|\eta\rangle, \tag{5}$$

where $\mathbf{Q}$ is an operator describing the optical system. Light generated at a source, represented by the vector $|U^{(i)}\rangle$, propagates a distance d to the sample then scatters, the scattered light passes through a lens and lastly the light propagates a distance d to the detector. This sequence of operations can be symbolically represented by the following expression

$$\mathbf{Q} = \mathbf{K}_d \mathbf{L} \mathbf{K}_d \mathbf{U}^{(i)}. \tag{6}$$

Here, the operator $\mathbf{K}_d$ is the operator for propagation through free space between two parallel planes separated by a distance d, the operator $\mathbf{L}$ represents the effect of an objective lens on the scattered field and the operator $\mathbf{U}^{(i)}$ is defined as $\int \mathrm{d}\mathbf{k}'_\parallel \mathrm{d}\mathbf{k}''_\parallel |\mathbf{k}'_\parallel\rangle\langle \mathbf{k}'_\parallel - \mathbf{k}''_\parallel | U^{(i)} \rangle \langle \mathbf{k}''_\parallel|$. Projecting Eq. (5) onto the coordinate basis yields

$$\langle r|S\rangle = \int \mathrm{d}^2 k'_\parallel \mathrm{d}^2 k_\parallel \mathrm{d}^2 r \, \langle r|k'_\parallel\rangle \langle k'_\parallel|\mathbf{Q}|k_\parallel\rangle \langle k_\parallel|r\rangle \langle r|\eta\rangle \tag{7}$$

For an incident plane wave, the kernel of the operator $\mathbf{Q}$ is approximated, by $\langle k'_\parallel|\mathbf{Q}|k_\parallel\rangle = \delta(k'_\parallel - k_\parallel)\Theta(k_\parallel)$, where $\Theta(k_\parallel)$ is a stepfunction that equals zero for spatial frequencies bigger than $NA \cdot k$. As expected, the lens acts as a bandpass filter. The sample is composed of a collection of N spheres with radius a_j and refractive index of m_j, where $1 \geq j \leq N$. Since $a_j \gg k$, each sphere is represented using a quasi-static approximation, i.e., $\langle r|\eta_j\rangle = \delta(r - r'_j)(ka_j)^3 \frac{m_j^2-1}{m_j^2+2}$. The particle response function for particle j is therefore given by $|S_j\rangle = \mathbf{Q}|\eta_j\rangle$ and the final field at the detector is $|S\rangle = \sum_{j=0}^{N} |S_j\rangle$. The field $\langle \mathbf{r}|S_j\rangle$ is called the particle response function (PRF) and is illustrated in Fig. 2 for a particle composed of SU-8 photoresist. Given the PRFs for M probes, the positions of these probes can then be determined from a hyperspectral image using nonlinear least-squares regression as described below.

A number of considerations arise in identifying the signal from individual probes in coherent scattering which are not encountered in fluorescence imaging. The structure and optical spectral responses of nanoprobes are coupled and the recorded spectra are generally different from the bulk material spectra. This happens because Mie scattering strongly couples the real and the imaginary parts of the refractive index. Compared to bulk material properties, the spectrum that would be recorded from spheres can be seen to additionally depend on the size of the

#187433 - $15.00 USD Received 20 Mar 2013; revised 2 May 2013; accepted 3 May 2013; published 17 May 2013

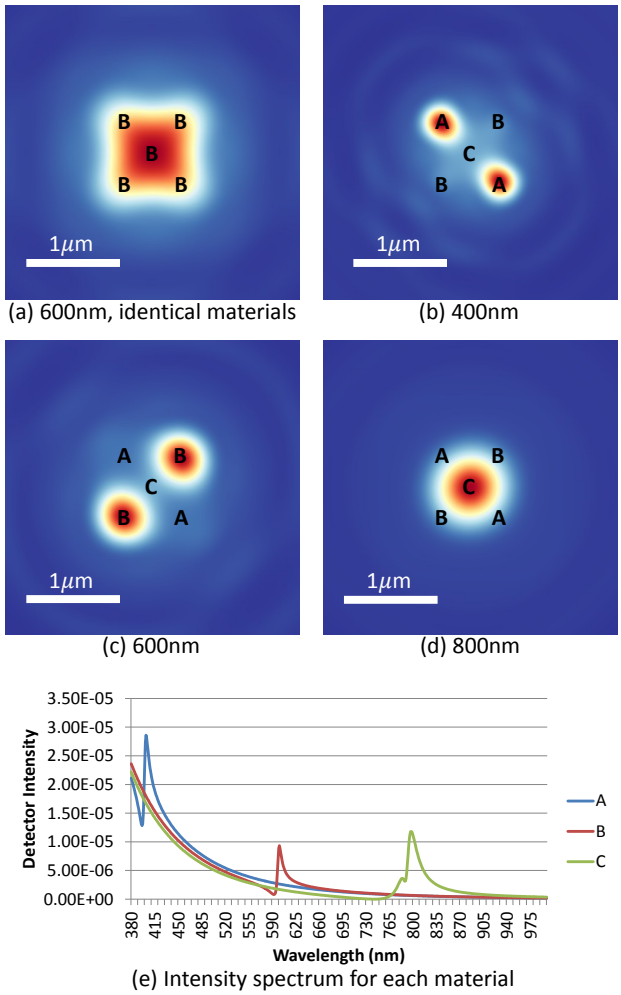

Fig. 3. Nanoprobes in a 5-point *die* arrangement imaged using coherent light in reflection. A, B, and C indicate the position and material of each probe. (a) The image produced at 600nm when all probes are made of the same material shows a single merged spot on the detector. (b-d) Probes composed of different materials can be separated spectrally. (e) The intensity spectrum of each probe is shown with resonance peaks at 400nm, 600nm, and 800nm respectively for materials A, B, and C.

#187433 - $15.00 USD Received 20 Mar 2013; revised 2 May 2013; accepted 3 May 2013; published 17 May 2013

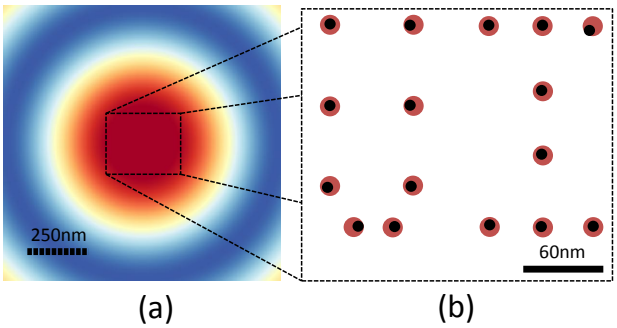

Fig. 4. Absorbance image of 16 spheres with a radius of 10 nm, the field of view is $1\mu\text{m} \times 1\mu\text{m}$. Nanoparticles material properties are specified using Lorentzian spikes with a FWHM of 25 nm.(a) The integrated intensity, the image that would be recorded with a conventional microscope. (b) Mapped locations of the spheres, after adding Gaussian noise to provide a SNR ≈ 10, the field of view is $0.25\mu\text{m} \times 0.2\mu\text{m}$. Black points show actual particle positions, and red circles are centered on reconstructed positions with 10nm confidence intervals. Particle positions are determined by fitting the complex PRF to the image, using the maximum intensity value at the resonance frequency as an initial estimate.

sphere and the parameters of the imaging system. The dependence on the size of the probes can be minimized by reducing the size of the nanoprobes well below the wavelength employed for imaging. Furthermore, we envision the use of nanoprobes whose spectral responses are perhaps overlapping but distinguishable by projecting the entire spectrum onto a set of appropriate basis functions. Since the contribution of each nanoprobe to the measured image depends in a non-separable manner on both frequency and position, the position of the nanoprobe and its signal must, in general, be estimated simultaneously. This may be accomplished by a number of iterative methods. For instance, starting with an initial guess of position, the forward model above may be used to predict the recorded fields and the ℓ^2 norm of the difference of the measured signal and the predicted one may be minimized with respect to the variation in the nanoprobe position. The signal at a nanoprobe resonant frequency is dominated by that nanoprobe. In the event that each nanoprobe is associated with an isolated peak in the spectrum, the identification of a single nanoprobe signal is simplified. This comes at the price of neglecting any data available at other frequencies, but it eliminates the need for an iterative process. Subsequently, the location of the corresponding nanoprobe may be determined, as is done in PALM/STORM, by finding the center of the intensity pattern at that frequency. This is illustrated in Fig. 3, which shows the image created by probes with varying material properties.

In Fig. 4, we demonstrate the potential for superresolved mapping using coherent scattering from nanoprobes. The absorbance image of 16 spheres with a radius of 10 nm each, all with distinct, nonoverlapping spectral responses, placed within the diffraction-limited focal spot is shown. The absorption peaks are arranged between wavelengths of 410 nm and 570 nm, separated by 11 nm intervals. This is the approximate range and spectral resolution achievable by varying the gold-silver ratio in alloy spherical nanoparticles [17], for example. The imaging system has a numerical aperture of 0.8. The nanoprobes are all unresolvable as may be seen from the image which appears as a single diffraction-limited spot. The signal from each nanoprobe is identified at its resonant frequency, as in Fig. 3 above. The position was estimated by finding the centroid of each signal by Gaussian fitting and mapped in Fig. 4(b). The resultant image matches the original distribution and forms the letters UI. The simulation was performed with a realistic SNR of 10, demonstrating the feasibility of the method.

#187433 - $15.00 USD Received 20 Mar 2013; revised 2 May 2013; accepted 3 May 2013; published 17 May 2013

2. Conclusion

We have described above a multiplex method in super-resolved imaging that offers large signals on short timescales and thus may be used to image dynamic systems. The technique described here is not tied to specific molecular transitions and may be scaled to spectral ranges convenient for specific applications. Nanoprobes may be distributed in prepared samples and may be attached to specific regions of interest. Functionalized nanoprobes find more and more biological applications [25]. Nanoprobes may be actively conjugated to specific molecular species in a manner similar to PALM/STORM or may be passively present along the contours of the imaged domain.

This coherent, spectral-domain method makes use of ideas developed in super-resolved fluorescent imaging in the time domain. The key idea across these modalities is the conversion of imaging into mapping of isolated probes. It can be seen here that isolating signals in the time domain is just one example in a much broader class of methods. We have presented a method to isolate signals from individual probes in the spectral domain. The examples given make use of nonoverlapping spectra, but a more general approach could accommodate identification of signals from probes with overlapping spectra by projective methods. Our analysis also suggests the possibility of using other channels, such as coherence or lifetime, to provide a means to identify the signals needed to map discrete probes. We have made use of absorbance images, but since the signals are coherently scattered, phase images could be obtained and used as well. In summary, our development of spectral domain super-resolution imaging can be easily generalized and will prove useful for a variety of imaging modalities.

Acknowledgments

The work was supported in part by the Beckman Institute for Advanced Science and Technology and by the National Science Foundation via grant CHE0957849.

#187433 - $15.00 USD Received 20 Mar 2013; revised 2 May 2013; accepted 3 May 2013; published 17 May 2013